HOSTED BY

ELSEVIER

Available online at www.sciencedirect.com

ScienceDirect

Journal of Magnesium and Alloys 3 (2015) 309–314
www.elsevier.com/journals/journal-of-magnesium-and-alloys/2213-9567

Full Length Article

Anisotropy of the crystallographic orientation and corrosion performance of high-strength AZ80 Mg alloy

Quantong Jiang [a], Xiumin Ma [a], Kui Zhang [b,*], Yantao Li [a,**], Xinggang Li [b], Yongjun Li [a], Minglong Ma [b], Baorong Hou [a]

[a] *Marine Corrosion and Protection Centre, Institute of Oceanology, Chinese Academy of Sciences, No. 7 Nanhai Road, Qingdao 266071, China*
[b] *State Key Lab for Non-ferrous Metals and Process, General Research Institute for Non-Ferrous Metals, Beijing 100088, China*

Received 23 September 2015; revised 10 November 2015; accepted 10 November 2015

Available online 2 December 2015

Abstract

A high-strength AZ80 Mg alloy was prepared through multi-direction forging, thermal extrusion, and peak-aged heat treatment. The microstructure, crystallographic orientation and corrosion performance of extrusion-direction, transverse-direction, and normal-direction specimens were investigated using scanning electron microscopy, electron backscatter diffraction, and atomic force microscopy, respectively. Experimental results showed that crystallographic orientation significantly influenced the corrosion performance of AZ80 Mg alloy. Corrosion rates largely increased with decreased (0 0 0 1) crystallographic plane intensity, whereas the (1 0 −1 0) and (2 −1 −1 0) crystallographic plane intensities increased. This study showed that the corrosion rates of alloy can be modified to some extent by controlling texture, thereby promoting the applications of high-strength AZ80 Mg alloys in the aerospace and national-defense fields.

Keywords: High-strength AZ80 Mg alloy; Anisotropy; Wrought; Crystallographic orientation; Corrosion performance; Surface energy

1. Introduction

Wrought magnesium alloys are attractive for aerospace and automotive industries because of their excellent properties [1]. However, the applications of wrought Mg alloys are hindered by their anisotropy caused by their strong texture [2–4]. Thus, texture analysis is an important tool for evaluating and understanding Mg-alloy performance [5–7]. Data on the correlation of texture with the corrosion behavior of AZ31 Mg alloys can be found in literature. Song et al. [8] found that AZ31 alloys exhibit corrosion anisotropy; their measured rolling surface (RS) is found to be more electrochemically stable and corrosion resistant than the cross-section surface (CS). Xin et al. [9,10] showed that the corrosion rate of AZ31 dramatically increases with decreased (0 0 0 1) texture intensity and increased (1 0 −1 0)/(1 1 −2 0) texture intensity. Shin and Song [11,12] demonstrated that the relationship between the corrosion performance of crystallographic planes and the different electrochemical activities of RS and CS surfaces originates from the different surface energy levels of the (0 0 0 1), (1 0 −1 0), and (1 1 −2 0) crystallographic planes. Wang et al. also concluded that the surface of an as-extruded AZ31 alloy bar with a high concentration of (1 0 −1 0) and (1 1 −2 0) oriented prism planes is more electrochemically stable and corrosion resistant than that with a high concentration of (0 0 0 2), (1 0 −1 0), and (1 1 −2 0) oriented planes [13].

High-strength AZ80 Mg alloys are widely used because of their relatively lower price and better mechanical properties than AZ31 alloys [14–16]. However, the relationship between crystallographic texture and corrosion performance of wrought AZ80 Mg alloys has never been reported. Knowledge on the relationship between the crystallographic orientation and corrosion rate of AZ80 alloys is important because it can guide process optimization to obtain the desirable texture for higher corrosion resistance.

* Corresponding author. State Key Lab for Non-Ferrous Metals and Process, General Research Institute for Non-Ferrous Metals, Beijing 100088, China. Tel: +86-10-82241168; fax: +86-10-82241168.
E-mail address: zhkui@grinm.com (K. Zhang).
** Corresponding author. Marine Corrosion and Protection Centre, Institute of Oceanology, Chinese Academy of Sciences, No. 7 Nanhai Road, Qingdao 266071, China. Tel: +86-532-82898832; fax: +86-532-82898832.
E-mail address: ytli@qdio.ac.cn (Y. Li).

http://dx.doi.org/10.1016/j.jma.2015.11.002
2213-9567/

In the present work, high-strength AZ80 Mg alloys were prepared through multi-direction forging, thermal extrusion, and peak-aged heat treatment. The microstructure, texture, and corrosion performance of extrusion-direction (ED), transverse-direction (TD), and normal-direction (ND) specimens were investigated. Texture evolution during the extruded processing of Mg alloys was further investigated to understand their effects on the anisotropy of anticorrosion properties. Corrosion rates were found to largely increase with decreased (0 0 0 1) crystallographic plane intensity and increased (1 0 −1 0) and (2 −1 −1 0) crystallographic plane intensity. The corrosion rates of alloys in the service environment can also be modified to some extent by controlling their texture, thereby promoting the applications of high-strength AZ80 Mg alloy in the aerospace and national-defense fields.

2. Experiments

The material initially used was an as-cast billet with an average composition of Mg–8.87A1–0.62Zn–0.15Mn–0.0034Fe–0.02Si (wt%). The billet (760 mm × 1250 mm) was homogenized at 410 °C for 24 h, treated by multi-direction forging at 350 °C–400 °C, and then extruded at 360 °C to a rectangular plate with dimensions of 230 mm × 140 mm (extrusion ratio = 10:3). Finally, the extrusion AZ80 alloy was peak aged at 175 °C for 24 h. The ED, TD, and ND specimens were cut from a peak-aged AZ80 alloy square rod (Fig. 1).

The texture and grain size of peak-aged AZ80 alloy coupons were determined by the electron backscatter diffraction (EBSD) technique. For the salt spray test, polarization-curve analysis, and AC impedance measurements, samples were molded into epoxy resin with only one side exposed as the available working surface. Their ND, TD, and ED surfaces were polished with up to 5000 grit SiC paper and then tested in 3.5 wt.% NaCl solution in salt spray [17]. Polarization curves and AC-impedance spectra were obtained with a Solatron 2273 system. Potentiodynamic scanning was performed at a rate of 0.5 mV/s after the cell was held at the open-circuit potential (OCP) for 400 seconds. Impedance was measured with the frequency ranged from 10,000 Hz to 0.1 Hz with 5 mV of amplitude of sinusoidal potential signals with respect to the OCP. After three days of salt spray in 3.5 wt.% NaCl, the specimens were cleaned in 200 g/LCrO_3 + 10 g/L $AgNO_3$ [18]. Atomic force microscopy (AFM) measurements of the detailed corrosion morphologies and pitting depth were imaged using an Agilent 5400 in tapping mode.

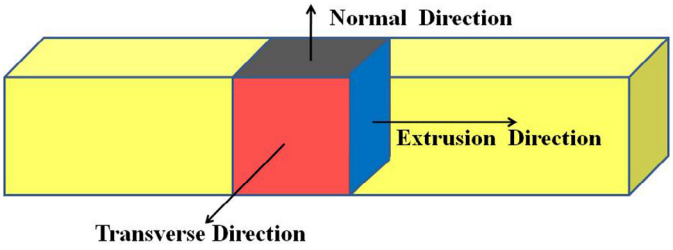

Fig. 1. The ED, TD, and ND specimens cut from a peak-aged AZ80 alloy square rod.

3. Results and discussion

3.1. Anisotropy of the microstructure and crystallographic orientation

The microstructures mainly consisted of primary α and eutectic precipitates (Fig. 2). Results showed that most grains recrystallized and that the originally deformed grains were depleted by the dynamic recrystallization grains. The average grain sizes of the three types of AZ80 specimens were similar, which implied that the grain-size difference was not responsible for the corrosion-rate difference among the different specimen types. A large amount of precipitates was observed to be distributed throughout the matrix for all specimens. The average sizes of these precipitates were slightly dispersed in morphology, whereas volume fraction was higher. These precipitates, as the cathode of electrochemical reactions, accelerated the corrosion process [19,20].

Actually, there was a difference at the volume fraction and distribution of $Mg_{17}Al_{12}$ phases in the three samples, and the volume fraction of precipitation phases in the ND sample showed the lowest value (Fig. 2). Then, the areas of the precipitated phases were counted by software (Image Pro Plus 6.0): (a) ND sample = 8.512%; (b) TD sample = 9.975%; (c) ED sample = 12.305%.

However, the distinction located that precipitated phases of the ED sample nearly connected into nets in many areas. In compassion with crystallographic orientations, the precipitated phases played a dual role in the corrosion resistance for aluminum-containing Mg alloys according to the classical theory of Song and Atrens [21]. The phases played dual roles that depended on the amount and distribution. The presence of the phase in the alloys could deteriorate the corrosion performance as it could act as an effective galvanic cathode. Otherwise, a fine and homogeneous phase appeared to be a better anti-corrosion barrier. Zhao et al. [22] also studied the relationship between the microstructure and precipitated phases of AZ91D alloy, which demonstrated that discrete precipitated phases preferentially accelerated the micro-galvanic corrosion process and then the interconnected precipitated phases improved the corrosion properties.

What's more, alloying magnesium with aluminum in general improves the corrosion resistance [23–25]. It is reported that the corrosion rate decreases rapidly with increasing aluminum up to 4%. Further aluminum additions up to 9% give only a modest further improvement. Most importantly, the beneficial role of aluminum was generally believed to be a result of β-phase precipitation, which has an important role as a corrosion barrier. In addition, the influence of the aluminum in increasing the corrosion resistance appears to be due to the aluminum altering the composition of the hydroxide film formed on the surface [26]. As shown in Fig. 2a and b, the $Mg_{17}Al_{12}$ phase precipitated was along the grain boundary, which would be as the cathode of electrochemical reactions to accelerate the corrosion process. But from the ED sample in Fig. 2c, an amount of the precipitated phase $Mg_{17}Al_{12}$ formed a continuous distribution in many areas on the grain boundaries, which were served as the corrosion barrier. Thus, the crystallographic

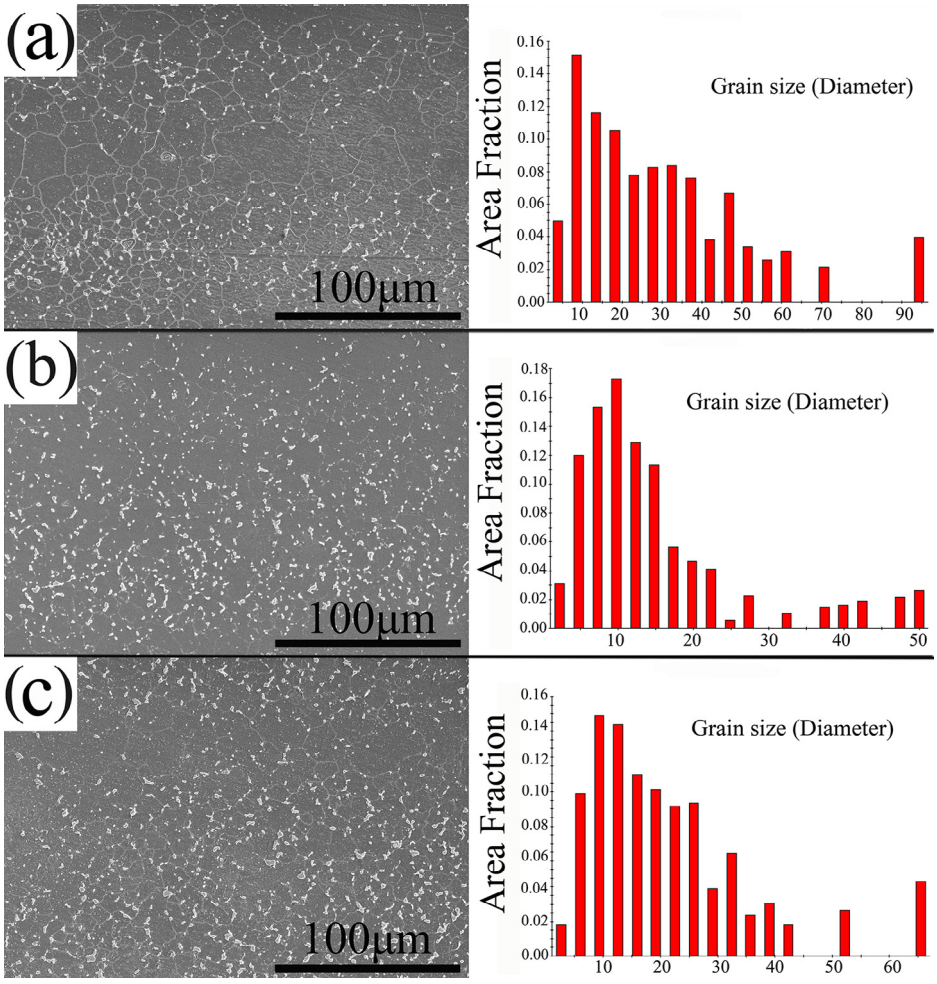

Fig. 2. Microstructures and grain sizes of high-strength AZ80 alloy: (a) ND specimen, (b) TD specimen, and (c) ED specimen.

orientations played a more important role than the precipitated phases in the corrosion resistance.

The microstructures of ND, TD, and ED specimens were examined by EBSD to understand the microstructure evolution during the process of wrought-alloy production (Fig. 3). The grain colors in the maps corresponded to the crystallographic axes shown in the inserted stereographic triangle. We determined that the (0 0 0 1) base planes of most grains were parallel to the ED. The c-axes of the grains were nearly normal to the exposed surface on the ND specimen. However, these results also confirmed that the TD and ED specimens mainly consisted of (1 0 −1 0) and (2 −1 −1 0) crystallographic plane intensities, respectively. This conclusion was consistent with the basal texture commonly reported for extrusion AZ80 alloy sheets [27].

3.2. Anisotropy of corrosion rates and surface morphologies

The corrosion rate of the specimens was calculated using $C = (W_0 - W_1)/S$, where C is the weight loss of metal because of corrosion ($g \cdot m^{-2}$), W_0 is the original weight (g), W_1 is the final weight without corrosion products (g), and S is the surface area (m^2). Each type had three specimens, so the corrosion rates were the average value. Fig. 4 shows that the ED specimens had the highest corrosion rate of 4.5259 $mg \cdot cm^{-2} \cdot d^{-1}$, whereas the ND specimens had the lowest at 2.6963 $mg \cdot cm^{-2} \cdot d^{-1}$. The corrosion rate followed the order ND < TD < ED, indicating that the ND surface of AZ80 Mg alloy square rod surface exhibited the highest corrosion resistance, whereas the ED surface had the lowest corrosion resistance.

Based on the above conditions, the relationship between corrosion rate and crystallographic plane was observed. Corrosion rate increased with decreased (0 0 0 1) crystallographic plane intensity and increased (1 0 −1 0) and (2 −1 −1 0) crystallographic plane intensities. This phenomenon can be due to the different crystallographic grain orientations having different electrochemical activities. A previous study on the relationship between corrosion rate and crystallographic plane energy has suggested that the activation energy for the dissolution of a densely packed surface is higher than that for the dissolution of a loosely packed one [28]. Song [8] theoretically proved that the energy of Mg (0 0 0 1), (1 0 −1 0), and (1 1 −2 0) surfaces is 1.808, 1.868, and 2.156 eV/nm^2, which can be

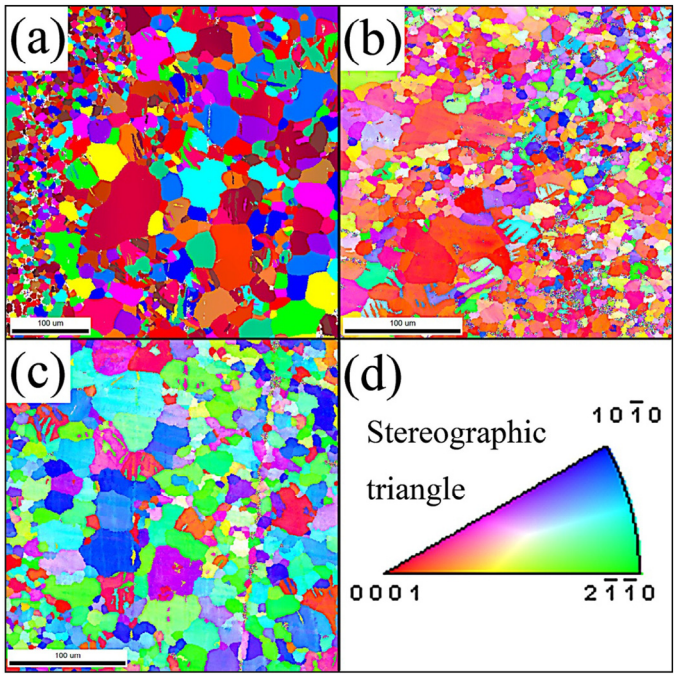

Fig. 3. Crystallographic orientation of high-strength AZ80 alloy obtained from EBSD analyses: (a) ND specimen, (b) TD specimen, and (c) ED specimen.

converted into 1.54×10^4, 3.04×10^4, and 2.99×10^4 J/mol, respectively. Thus, the (0 0 0 1) crystallographic plane has the lowest surface energy and should dissolve slower than the (1 0 −1 0) and (1 1 −2 0) crystallographic planes. According to the hexagonal close-packed (hcp) structure of Mg, (1 1 −2 0) and (2 −1 −1 0) crystallographic planes both belong to the same crystal family, so they have the same crystallographic intensity, surface energy, and electrochemical activity. Therefore, the NS surface mainly consisted of (0 0 0 1), whereas the TD and ED surfaces mainly comprised (1 0 −1 0) and (2 −1 −1 0) crystallographic planes.

After salt-spray exposure, the corrosion products that formed on the specimen surfaces were removed by pickling. A

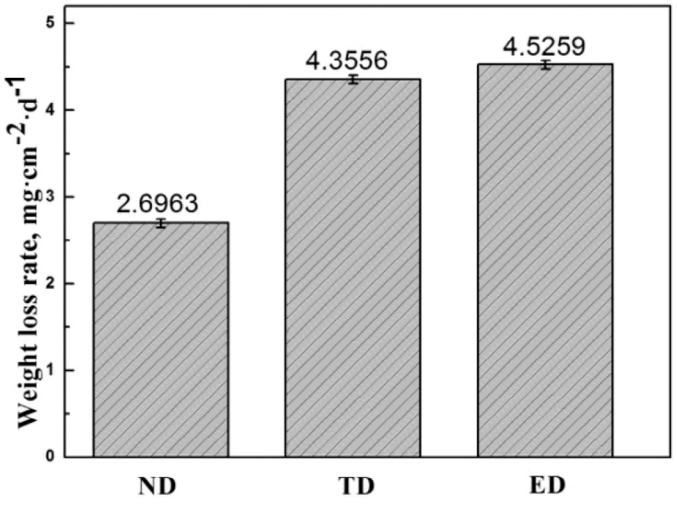

Fig. 4. Weight-loss rates of specimens sprayed with 3.5% NaCl for 3 days.

slight corrosion attack occurred horizontally between the matrix and precipitates of ND specimen, as shown in Fig. 5a, whereas corrosion-damage patterns were irregularly distributed over the TD (Fig. 5b) and ED (Fig. 5c) specimens. This finding further proved that crystallographic texture determined the corrosion rate. Thus, corrosion pits increased because of the decrease in (0 0 0 1) and increase in (1 0 −1 0)/(2 −1 −1 0) crystallographic planes. This phenomenon was due to the micro-galvanic effect resulting in a preferential corrosion of (1 0 −1 0) and (2 −1 −1 0) oriented grains.

3.3. Anisotropy of electrochemical characteristics

The OCP was found to be comparatively stable before measurement. Moreover, a corrosion product film formed on the specimen surfaces, and no clear localized corrosion occurred. The cathodic Tafel slopes were similar among specimens under different conditions, which indicated that hydrogen evolution occurred [29].

Interestingly, the polarization curves (Fig. 6) showed that ND surface had a more positive OCP than other surfaces. In other words, the OCP of the closely packed (0 0 0 1) crystallographic plane was more positive than that of the less densely packed (1 0 −1 0)/(2 −1 −1 0) crystallographic planes. Thus, electrochemical activity followed the order (0 0 0 1) > (1 0 −1 0) > (2 −1 −1 0), meaning that the high-strength AZ80 Mg alloy had a strong corrosion-resistance anisotropy mainly dependent on the crystallographic grain orientation. According to a previous study, the relationship between grain orientation and corrosion performance can be indicated by the activation energy for crystallographic-plane dissolution. Furthermore, atoms in lower-surface-energy planes dissolved relatively more slowly [30].

In theory, the electrochemical corrosion rate of the Mg alloy can be calculated by $I_\alpha = nFk \exp[(Q + \alpha nFE)/RT]$, where n is the number of electrons involved in the reaction; k is a reaction constant; F, R, T, E and α are Faraday constant, gas constant, absolute temperature, electrode potential, and transit coefficient, respectively; and Q is the activation energy for a metallic ion to escape from the metal lattice and dissolve into the solution [10]. Song [8] indicated that the ratio of the anodic dissolution rate $I_\alpha^{(k,l,m,n)}$ of a crystallographic plane over that $I_\alpha^{(0,0,0,1)}$ of the base plane should be $\frac{I_\alpha^{(k,l,m,n)}}{I_\alpha^{(0,0,0,1)}} = \exp\left\{\frac{\alpha\left[Q^{(k,l,m,n)} - Q^{(0,0,0,1)}\right]}{RT}\right\}$. If $\alpha = 1/2$, after using the theoretical calculated surface energy values for Mg (0 0 0 1), (1 0 −1 0), and (2 −1 −1 0), then $\frac{I_\alpha^{(10\bar{1}0)}}{I_\alpha^{(0,0,0,1)}} = \exp\left\{\frac{1/2[30400-15400]}{8.31\times298}\right\} \approx 20$ and $\frac{I_\alpha^{(2\bar{1}\bar{1}0)}}{I_\alpha^{(0,0,0,1)}} = \exp\left\{\frac{1/2[29900-15400]}{8.31\times298}\right\} \approx 18$, respectively. Therefore, the corrosion rates of the (1 0 −1 0) and (2 −1 −1 0) crystallographic planes were higher than those of the base plane (0 0 0 1).

In addition to the influence on anodic dissolution, crystallographic-plane energy also indirectly affected the cathodic hydrogen evolution. A higher-energy crystallographic

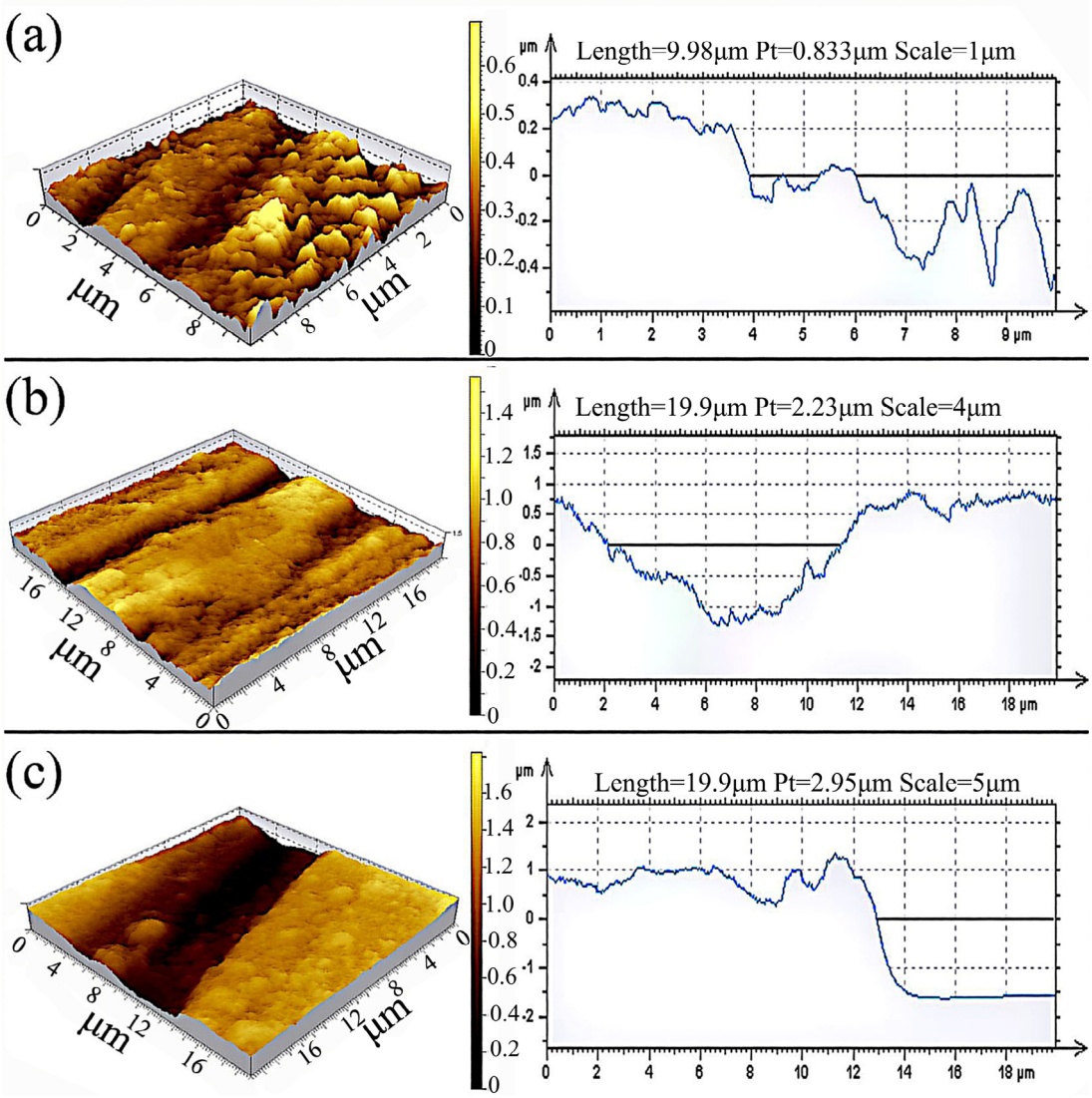

Fig. 5. Surface morphologies and depth of corrosion pits obtained from AFM analyses: (a) ND specimen, (b) TD specimen, and (c) ED specimen.

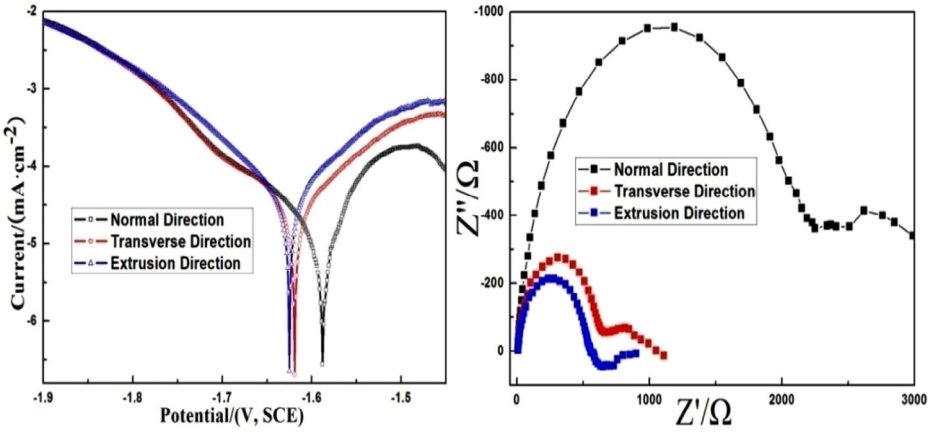

Fig. 6. Polarization curves and AC impedance of specimens measured in 3.5% NaCl solution.

plane enabled a higher density of hydrogen-adsorption sites, which benefited water or proton adsorption and accelerated the hydrogen reaction. Therefore, a closely packed plane with a higher surface energy can have a better catalytic effect on hydrogen reduction, which explained the higher cathodic current density of ED than TD and ND in the polarization curves. However, the influence of surface energy was indirect and thus had a less significant effect on the activation energy for hydrogen reaction than on that for Mg dissolution. Therefore, the difference in cathodic current density among ND, TD, and ED was less than that in anodic current density.

4. Conclusion

(1) A high-strength AZ80 Mg alloy was prepared through multi-direction forging, thermal extrusion, and peak-aged heat treatment. The ND surface of an AZ80 square rod mainly consisted of a closely packed (0 0 0 1) crystallographic plane with low surface energy. A amount of the precipitated phase $Mg_{17}Al_{12}$ formed of TD and ND samples was along the grain boundary, which would be as the cathode of electrochemical reactions to accelerate the corrosion process. Amounts of precipitated phases of ED sample formed a continuous distribution in many areas, which played a role in the corrosion barrier. The crystallographic orientations played a more important role than the precipitated phases in the corrosion resistance. Thus, Nd sample's anodic dissolution and cathodic hydrogen evolution were more difficult than those of TD and ED surfaces, wherein most grains had (1 0 −1 0) and (2 −1 −1 0) orientations, respectively.

(2) The corrosion rate of different crystallographic planes of AZ80 Mg alloy was estimated based on an electrochemical-dissolution-rate equation. Findings indicated that the theoretical dissolution rates of crystallographic planes were as follows: (0 0 0 1) > (1 0 −1 0) > (2 −1 −1 0).

(3) Different locations in the interior of the AZ80 alloy billet were subjected to different stresses and strains in multi-direction forging and thermal extrusion. Given the low symmetry of the hcp crystal structure, the AZ80 alloy square rod showed evident anisotropy in different directions and influenced corrosion performance. The crystallographic grain orientations played an important role, which indicated that material performance can be modified to some extent by controlling texture. All these results can help expand the applications of high-strength AZ80 alloys in the aerospace and national-defense fields.

Acknowledgement

The authors gratefully acknowledge the National Natural Science Foundation of China (grant no. 51501181) and Professor Liu for providing support for this work.

References

[1] E.A. Ball, P.B. Prangnell, Script. Mater. 31 (2) (1994) 111–116.
[2] J. Yuan, K. Zhang, T. Li, X. Li, Y. Li, M. Ma, et al., Mater. Des. 40 (2012) 257–261.
[3] J. Bohlen, M.R. Nürnberg, J.W. Senn, D. Letzig, S.R. Agnew, Acta Mater. 55 (6) (2007) 2101–2112.
[4] M. Liu, D. Qiu, M.C. Zhao, G. Song, A. Atrens, Script. Mater. 58 (5) (2008) 421–424.
[5] T. Zhang, G. Meng, Y. Shao, Z. Cui, F. Wang, Corros. Sci. 53 (9) (2011) 2934–2942.
[6] F. Kaiser, J. Bohlen, D. Letzig, K.U. Kainer, A. Styczynski, C. Hartig, Adv. Eng. Mater. 5 (12) (2003) 891–896.
[7] Q. Zhang, H. Guo, F. Xiao, L. Gao, A.B. Bondarev, W. Han, J. Mater. Process. Technol. 209 (15) (2009) 5514–5520.
[8] G.L. Song, R. Mishra, Z.Q. Xu, Electrochem. Commun. 12 (8) (2010) 1009–1012.
[9] R.L. Xin, B. Li, L. Li, Q. Liu, Mater. Des. 32 (8) (2011) 4548–4552.
[10] R.L. Xin, M.Y. Wang, J.C. Gao, P. Liu, Q. Liu, Mater. Sci. Forum 610 (2009) 1160–1163.
[11] K.S. Shin, M.Z. Bian, N.D. Nam, JOM (1989) 64 (6) (2012) 664–670.
[12] G.L. Song, Z. Xu, Corros. Sci. 63 (2012) 100–112.
[13] B.J. Wang, D.K. Xu, J.H. Dong, W. Ke, Script. Mater. 88 (2014) 5–8.
[14] H. Yu, S.H. Park, B.S. You, Mater. Sci. Eng. A Struct. Mater. 610 (2014) 445–449.
[15] Z. Cao, F. Wang, Q. Wan, Z. Zhang, L. Jin, J. Dong, Mater. Des. 67 (2015) 64–71.
[16] X. Huang, K. Suzuki, N. Saito, Mater. Sci. Eng. A Struct. Mater. 508 (1) (2009) 226–233.
[17] Q.T. Jiang, K. Zhang, X.G. Li, Y. Li, M. Ma, G. Shi, et al., J. Magnes. Alloys 1 (3) (2013) 230–234.
[18] Q.T. Jiang, M.L. Ma, K. Zhang, X. Li, Y. Li, G. Shi, et al., J. Rare Earths 32 (12) (2014) 1170–1174.
[19] D. Zhao, Z. Wang, M. Zuo, H. Geng, Mater. Des. 56 (2014) 589–593.
[20] Q.T. Jiang, K. Zhang, X.G. Li, Y.J. Li, M.L. Ma, G.L. Shi, et al., Corros. Eng. Sci. Technol. 49 (7) (2014) 651–655.
[21] G. Song, A. Atrens, Adv. Eng. Mater. 1 (1) (1999) 11–33.
[22] M. Zhao, M. Liu, G. Song, A. Atrens, Corros. Sci. 50 (2008) 1939–1953.
[23] K. Nisancioglu, O. Lunder, T.R. Aune, Corrosion mechanism of AZ91 magnesium alloy. Past to Future: 47th Annual World Magnesium Conference. 1990, pp. 43–50.
[24] G.L. Makar, J. Kruger, J. Electrochem. Soc. 137 (2) (1990) 414–421.
[25] C.B. Baliga, P. Tsakiropoulos, Mater. Sci. Technol. 9 (6) (1993) 513–519.
[26] W.S. Loose, L.M. Pidgeon, J.C. Mathes, N.E. Woldmen, Corrosion and Protection of Magnesium, ASM International, Materials Park, OH, 1946, pp. 173–260.
[27] B.Q. Shi, R.S. Chen, W. Ke, Mater. Sci. Eng. A Struct. Mater. 546 (2012) 323–327.
[28] J.J. Gray, B.S. El Dasher, C.A. Orme, Surf. Sci. 600 (12) (2006) 2488–2494.
[29] A.D. Sudholz, K. Gusieva, X.B. Chen, B.C. Muddle, M.A. Gibson, N. Birbilis, Corros. Sci. 53 (6) (2011) 2277–2282.
[30] G.L. Song, Z.Q. Xu, Electrochim. Acta 55 (13) (2010) 4148–4161.